HOKKAIDO UNIVERSITY

Title	Nanowire-structured titanate with anatase titania : Characterization and photocatalytic activity
Author(s)	Amano, Fumiaki; Yasumoto, Taikei; Shibayama, Tamaki et al.
Citation	Applied Catalysis B : Environmental, 89(3-4), 583-589 https://doi.org/10.1016/j.apcatb.2009.01.013
Issue Date	2009-07-15
Doc URL	https://hdl.handle.net/2115/44873
Type	journal article
File Information	ACB89-3-4_583-589.pdf

Hokkaido University Collection of Scholarly and Academic Papers : HUSCAP

Nanowire-Structured Titanate with Anatase Titania: Characterization and Photocatalytic Activity

Fumiaki Amano,*[a,b] Taikei Yasumoto,[b] Tamaki Shibayama,[c] Satoshi Uchida[d] and Bunsho Ohtani[a,b]

[a]Catalysis Research Center, Hokkaido University, Sapporo 001-0021, Japan. Tel: +81-11-706-9132, Fax: +81-11-706-9133

[b]Graduate School of Environmental Science, Hokkaido University, Sapporo 060-0810, Japan.

[c]Center for Advanced Research of Energy Conversion Materials, Hokkaido University, Sapporo 060-8628, Japan.

[d]Research Center for Advanced Science and Technology, The University of Tokyo, Tokyo 153-8904, Japan.

*corresponding author, E-mail: amano@cat.hokudai.ac.jp

Abstract

Nanowire-structured titanate with titanium(IV) oxide (titania) was obtained by calcination of potassium ion-containing titanate nanowires prepared through alkali treatment of titania nanoparticles. The presence of potassium ions in the as-synthesized titanate nanowires was required for maintenance of the nanowire structure under the conditions of post heat treatment. The crystallite structure, composition, morphology, specific surface area, pore volume distribution, and optical properties were found to be dependent on the temperature at which titanate nanowires were calcined. Photocatalytic activity was examined using three probe reactions: oxidative decomposition of acetic acid in an aqueous solution, oxygen liberation from an aqueous silver sulfate solution, and hydrogen liberation from an aqueous methanol solution in the presence of hexachloroplatinic acid as a precursor of photodeposition of platinum particles. Detailed characterization and results of photocatalytic activity tests revealed that titanate crystallites greatly contributed to the photocatalytic activities of the calcined nanowires except for photocatalytic hydrogen liberation. It was found that platinum was preferentially photodeposited on anatase crystallites rather than on titanate crystallites for hydrogen liberation.

1. Introduction

In the past several decades, a number of papers on photocatalysis by titanium(IV) oxide (titania; TiO_2) have been published. Through these studies, it has been clarified that different titania particles or films prepared from different sources or by different fabrication methods exhibit different photocatalytic activities and also that the order of photocatalytic activity strongly depends on the reactions and their conditions. The former fact suggests that photocatalytic activity cannot be explained by using a simple function of composition or weight of photocatalysts. This is the reason why we believe that there is a reasonable correlation between structural characteristics and photocatalytic activity of samples. However, it is impossible, in principle, to change or adjust one structural characteristic with the others unchanged, and clarification of the effect of one structural characteristic, such as particle size or particle shape, on photocatalytic activity is very difficult and has not been reported. Therefore, we must continue studies for clarification of the structure-activity correlation and, in order to extend basic knowledge, development of photocatalyst materials having non-spherical morphology of particular shapes, such as wires, rods, and platelets is important.

As an example of non-spherical structured photocatalysts, Kasuga et al. have reported the synthesis of titania nanotubes by alkaline treatment of titania particles at around 383 K followed by neutralization of alkali titanate nanotubes [1,2]. The as-synthesized nanotubes are not composed of anatase titania but of sodium titanate or titanic acid [3]. Crystallization of nanotubes to anatase crystallites by calcination or hydrothermal treatment often resulted in conversion of the tubes into wires [4,5] and particles [6-8]. On the other hand, titanate nanowires, without inner void space, can be synthesized by hydrothermal treatment at a higher temperature than that used for titanate nanotube synthesis, and nanowires composed of monoclinic TiO_2(B) and anatase crystallites were synthesized by heat treatment of the thus-prepared sodium titanate nanowires [7]. Such a wire structure is expected to show higher thermal stability than that of the tube structure. Substitution of sodium hydroxide with potassium hydroxide gave, as expected, potassium titanate nanowires with a composition of $K_2Ti_6O_{13}$ or $K_2Ti_8O_{17}$ [9-11].

One of the authors (SU) also synthesized potassium titanate nanowires by hydrothermal treatment [12]. The content of potassium ions was low since they were removed by washing with water and neutralization with acidic solutions. It is therefore expected that nanowires will be transformed into

titania nanowires of anatase crystallites by post heat treatment. It has often been reported that nano-sized anatase titania particles with high crystallinity show relatively high photocatalytic activity for oxidative decomposition of organic compounds due to the large surface area enhancing the adsorption of substrate molecules and the lesser recombination of photoexcited electrons and holes [13,14]. Indeed, anatase crystallites with nanotube, nanowire (nanofiber), and nanobelt (nanoribbon) structures seemed to exhibit photocatalytic activity higher than that of commercial titania nanoparticles such as Degussa P25 [4,5,15]. However, the reason(s) for the higher photocatalytic activity, if it is appreciable, could not be clarified and the advantage of the non-spherical morphology has not yet been revealed.

In the present study, we prepared nanowire-structured photocatalysts by calcination of titanate nanowires containing potassium ions. The photocatalytic activities of calcined nanowires were investigated from various viewpoints using three photoreactions. The properties that influence the photocatalytic activity of nanowire-structured composites of anatase and titanate crystallites are discussed on the basis of results of detailed characterization and probe reaction tests.

2. Experimental

2.1. Preparation

Titania nanoparticles, P25 supplied by Nippon Aerosil, were hydrothermally treated with a 17-mol L^{-1} potassium hydroxide solution in a pressure-tolerant Teflon bottle at 383 K for 20 h. The resulting precipitate was washed and neutralized using deionized water and an aqueous acetic acid solution, respectively. After freeze-drying, thus-obtained titanate nanowires were calcined in air at various temperatures (673–973 K) for 1 h. The calcined samples are denoted as TNW*x*, in which *x* means the calcination temperature in the unit of K, and TNW0 is used to denote titanate nanowires without calcination. Potassium tetratitanate ($K_2Ti_4O_9$) and potassium hexatitanate ($K_2Ti_6O_{13}$) were prepared by solid-state reaction of a stoichiometric mixture of potassium carbonate and titania at 1173 K for 24 h [16].

2.2 Characterization

Morphology of the samples was observed by a field-emission type scanning electron microscope (FE-SEM; JEOL JSM-7400F) and a transmission electron microscope (TEM; JEOL JEM-2010F). The chemical composition was analyzed by a JEOL JED-2300 energy dispersive X-ray spectrometer (EDS) equipped in the SEM (JEOL JSM-6360LA). X-ray diffraction (XRD) patterns were recorded on a Rigaku RINT ULTIMA diffractometer with Cu K_α radiation. Brunauer-Emmett-Teller (BET) specific surface area was determined from nitrogen adsorption at 77 K on a Yuasa Ionics NOVA 1200e surface area and pore size analyzer. Pore volume distribution was estimated from the desorption isotherm recorded on the analyzer using the Barret-Joyner-Halenda (BJH) method. Before surface area and pore volume distribution analyses, the samples were heated at 423 K under vacuum for 1 h. The diffuse-reflection electronic absorption spectra were recorded using barium sulfate as a standard material with a Hamamatsu Photonics PMA-11 analyzer.

2.3. Photocatalytic activity

Photocatalytic activity of the samples was evaluated by three kinds of photocatalytic reactions in aqueous solutions: (a) oxidative decomposition of acetic acid under aerated conditions, (b) oxygen (O_2) liberation from water in the presence of silver sulfate as a sacrificial agent, and (c) hydrogen (H_2) liberation from an aqueous methanol solution, with the following stoichiometries [17,18].

(a) $CH_3COOH + 2O_2 \rightarrow 2CO_2 + 2H_2O$

(b) $4Ag^+ + 2H_2O \rightarrow 4Ag + O_2 + 4H^+$

(c) $CH_3OH \rightarrow HCHO + H_2$

Each photocatalyst powder (50 mg) was suspended in an aqueous solution (5.0 cm^3) containing (a) 5.0 vol% acetic acid, (b) 25 mmol L^{-1} silver sulfate, or (c) 50 vol% methanol and irradiated under (a) air or (b and c) argon with magnetic stirring (1000 rpm). The concentration of powders in a suspension was relatively high enough to prevent a transmission of light. The suspensions of (b) and (c) were bubbled with Ar before irradiation. Photoirradiation (> 290 nm) was performed using a 400-W high-pressure mercury lamp (Eiko-sha) at 298 K. In the case of reaction (c), hexachloroplatinic acid ($H_2PtCl_6 \cdot 6H_2O$), which is reduced *in situ* to platinum metal deposits by photoexcited electrons, was added before photoirradiation (0.1 wt% unless otherwise stated). The molar amount of liberated (a)

carbon dioxide (CO_2), (b) O_2, or (c) H_2 in the gas phase of the reaction mixture was measured using a TCD-gas chromatograph (Shimadzu GC-8A) equipped with MS-5A and Porapak-Q columns. The molar amount was calibrated considering the increase of the pressure in the reactor by increase of the gas-phase molecules. The rate of O_2 liberation in reaction (b) tends to decrease with irradiation time due to the pH decrease by stoichiometric proton liberation resulting in depletion of adsorption of silver cation [19].Therefore, photocatalytic activity was estimated from the initial rate of O_2 evolution. For the other reactions, the rate of linear increase in product yield was used for estimation of photocatalytic activity, except for reaction (c) over P25 in the low loading region of platinum.

3. Results and Discussion

3.1. Morphology and composition

Figure 1a shows TEM image of as-synthesized titanate nanowires (TNW0). The structure was not tubular; absence of inner void space was confirmed. Lattice fringes corresponding to interlayer spacing of the layered structure were clearly observed. The rest of Fig. 1 shows FE-SEM images of TNW0 and samples calcined at various temperatures. TNW0 exhibited a fibrous structure with a typical diameter of 5–15 nm and a length of several hundreds of nanometers. The nanowires seemed to be bundled, which were further aggregated to form secondary large particles of a few micrometers. After calcination at a temperature below 773 K, change in the size of nanowires was negligible, while the bundle of nanowires seemed to be raveled out partly. Heat treatment at 873 K increased the diameter of the nanowires to 20–30 nm and decreased the length to a few hundred nanometers (Fig. 1d). The wire-like nanostructure was maintained without appreciable change in morphology even after calcination at 973 K (Fig. 1e), though small particles (20–40 nm) as well as wires were observed (Fig. 1f).

Figure 2 shows XRD patterns of samples. TNW0 exhibited a pattern with less intense broad peaks. The pattern resembled previously reported patterns for potassium titanate nanowires synthesized by hydrothermal treatment at higher temperatures (403–473 K) for longer times (2–4 days) compared with the conditions used for the present nanowire preparation [9-11]. The peak located at ca. 12 degree is assignable to the interlayer spacing of titanate nanowires. Many polymorphs of potassium titanates, $K_2Ti_nO_{2n+1}$, of different crystallite structures, such as layer (n = 2 and 4) and tunnel (n = 6 and 8),

have been reported [20]. Heat treatment in air at < 773 K induced no appreciable change in the XRD patterns. When the temperatures was increased to 873 K, peaks assigned to anatase crystallites appeared, while the nanowire structure still remained as depicted in Fig.1d. Another additional crystal phase, potassium hexatitanate ($K_2Ti_6O_{13}$) with a tunnel structure, was also observed in the XRD pattern of TNW973. It has been reported that a partially protonated potassium tetratitanate, $K_{1.33}H_{0.67}Ti_4O_9$, is transformed to hexatitanate by calcination [20]. On the other hand, decomposition of $K_2Ti_8O_{17}$ nanowires to $K_2Ti_6O_{13}$ and anatase titania at temperatures of 873–1073 K has been reported [5].

Figure 3 shows high-resolution TEM images indicating the presence of nanowire-structured composites of anatase titania and layered titanate in TNW873. Lattice fringes of anatase titania (d_{101}=0.35 nm) were found in some of the wires. Fringes corresponding to lattice spacing of ca. 0.83 nm were more frequently observed in wires. Although the interlayer spacing (d_{200}) of $K_2Ti_4O_9$ is 0.88 nm, it is known that the interlayer spacing is modified depending on the extent of proton exchange and water intercalation [16, 20]. Thus, the observed 0.83 nm distance is attributable to interlayer spacing of layered tetratitanate. The composition of the as-synthesized nanowires is thought to be $K_{0.74}H_{1.26}Ti_4O_9$ on the basis of results of EDS analyses (the molar ratio of Ti/K was estimated to be 5.4), if it is composed of a single layered tetratitanate. The molar ratio of Ti/K for TNW973 was estimated to be 6.1, indicating that the molar ratio of $K_2Ti_6O_{13}/TiO_2$ could be estimated to be 14/86, assuming that TNW973 is a simple mixture of $K_2Ti_6O_{13}$ and TiO_2.

It should be noted that washing with 1.0 mol L^{-1} hydrochloric acid decreased the thermal stability of nanowires. Calcination of this potassium-poor sample at 973 K resulted in collapse and conversion of the wire-like structure into spherical particles. This implies that potassium ions significantly contribute in maintenance of the nanowire structure. Therefore, the small spherical particles in TNW973 would not be potassium titanate. It is concluded that calcination at 873 K converts a part of layered tetratitanates into anatase titania without drastic change in the wire-structured morphology, and tunnel-structured $K_2Ti_6O_{13}$ was generated in addition to anatase titania at > 973 K.

3.2. Surface area and pore structure

Figure 4 shows the effect of calcination temperature on the BET specific surface area of samples. The starting nanowires, TNW0, exhibited relatively large surface area, 330 m^2g^{-1}. The surface area gradually decreased with elevation of calcination temperature up to 773 K and significantly decreased when anatase crystallites were formed at 873 K. However, TNW873 still exhibited a large surface area, 78.4 m^2 g^{-1}, presumably due to its wire-like structure.

The nitrogen adsorption/desorption isotherms of TNW0 were type II with a type H1 hysteresis loop at high relative pressure according to IUPAC classifications [21]. Figure 5 shows the pore volume distribution calculated from the desorption part using the BJH method. The broad peak positioned in the range of 8-30 nm is probably caused by aggregation of nanowires [8,9]. The pore volume and the size of the samples are summarized in Table 1. They were gradually increased by increasing the temperature up to 773 K. The pore diameter was roughly consistent with the aperture size in the secondary particles of the aggregated nanowires observed by FE-SEM images (Fig. 1e). At higher temperatures (> 973 K), the pore volume was drastically decreased by calcination because of growth of the wires and formation of small spherical particles. It was concluded that calcined nanowires having potassium ions exhibited a larger surface area and higher pore volume even after calcination at around 873 K. The pore property was changed in the same way as the morphology.

3.3. Optical properties

Diffuse-reflection electronic absorption spectra were measured in order to evaluate electronic band structure of the nanowires (Fig. 6). The photoabsorption edge of titania located at around 380 nm corresponds to band-gap transition from the valence band mainly composed of O 2p orbitals to the conduction band of Ti 3d orbitals. Assuming indirect allowed transition, band-gap energy (E_g) was determined by an intercept of a straight line fitting to the rise of a plot of $[F(R_\infty)\ h\nu]^{0.5}$ against $h\nu$, where $F(R_\infty)$ is Kubelka-Munk function and $h\nu$ is the incident photon energy [22]. TNW0 showed E_g of 3.35 eV as shown in Table 1. The energy was slightly red-shifted by calcination at 673 K and reached 3.23 eV at 773 K. It is clear from FE-SEM observation that the shift could not be attributed to growth of the wires. This indicates that the relatively large E_g of TNW0 is not induced by a quantum size effect but by change in the composition. The rise of a plot of $[F(R_\infty)\ h\nu]^{0.5}$ against $h\nu$ for P25 was

fitted by two straight lines. The E_g values of 3.21 and 3.04 eV in P25 correspond to the band gaps of anatase and rutile, respectively. The E_g of TNW773 resembles that of anatase titania rather than the as-synthesized nanowires, though its XRD pattern contained no anatase peaks. The diffraction peak at around 24-25 degrees of TNW773 was positioned between the peak of anatase titania (101) at 25.3 degrees and the peak of TNW0 (Fig. 2). It is noted that E_g values of TNW773, TNW873 and TNW973 were almost same, suggesting that the electronic structure of as-synthesized nanowires was considerably changed even at 773-K calcination.

3.4. Photocatalytic reactions

Figure 7 shows the results of photocatalytic O_2 liberation from water in the presence of silver ions as a sacrificial agent. It has been shown by quantitative analysis of defects using methylviologen that titania powders having few crystalline defects are appropriate for this type of reaction [18]. The nanowires without calcination, TNW0, showed a very low rate of O_2 liberation. The photocatalytic activity of samples gradually increased with an increase in calcination temperature. Calcination at < 773 K caused a gradual decrease in specific surface area and disappearance of small pores. Since there was no appreciable change in morphology, the decrease and the disappearance might be related to annealing of the surface defects of nanowires. It is known that crystalline defects of a photocatalyst work as centers of photoinduced electron-hole recombination. Thus, one of the reasons for the activity increase would be decrease in surface and bulk defects of nanowires by calcination. Samples calcined at > 873 K showed the highest activity among the nanowires, and the photocatalytic activity for O_2 liberation of TNW773 was higher than that of $K_2Ti_4O_9$ and $K_2Ti_6O_{13}$. However, their photocatalytic activity levels were less than that of P25 composed of mainly anatase and rutile.

Figure 8 shows the results of photocatalytic oxidative decomposition of acetic acid under aerated conditions. Acetic acid has several merits as a probe molecule for the test of photocatalytic activity, e.g., fewer intermediates than that in decomposition of dyes and liberation of CO_2 into the gas phase due to the solution acidity [23]. TNW0 with a large surface area showed appreciable activity for decomposition of acetic acid, in contrast to the low level of activity for photocatalytic O_2 liberation by water oxidation. This might indicate that a large surface area has a significant effect in the former reaction. The photocatalytic activity level of titanate nanowires was gradually increased by

increasing the calcination temperature. Therefore, properties affecting the activity were not only the specific surface area but also the amount of defects on surface and in bulk. Although a decrease in crystalline defects was a trade-off for a decrease in specific surface area in the present nanowires, TNW973 exhibited a level of photocatalytic activity higher than that of P25. The high level of activity would mainly be due to the small amount of crystalline defects of both titanates and anatase titania.

Figure 9 shows the results of photocatalytic H_2 liberation from an aqueous methanol solution in the presence of *in-situ* deposited platinum. The amount of chloroplatinic acid added to the reaction mixture corresponded to 0.1 wt% platinum loading. Linear increase of H_2 liberation was observed except for P25, over which the rate of H_2 liberation decreased with irradiation time and reached at steady state after 40-min irradiation. The negligible induction period over every sample indicates fast photocatalytic reduction of platinum precursor. TNW0 showed H_2 liberation rate comparable to that of P25 in such a low platinum loading region. The activity for H_2 liberation was almost constant for the samples calcined at < 773 K. Heat treatment of nanowires at > 873 K markedly enhanced the photocatalytic activity accompanied by generation of anatase titania crystallites. This clearly shows that the presence of anatase crystallite has a significant effect on this type of photocatalytic reaction rather than specific surface area and crystalline defects.

3.5. Effect of platinum loading on nanowire photocatalyst

Figure 10 shows the rate of photocatalytic H_2 liberation as a function of the amount of *in-situ* deposited platinum. In the absence of chloroplatinic acid, there was negligible H_2 liberation from every sample. TNW973 exhibited a much higher rate of H_2 liberation than that of P25 in the low loading region (< 0.4 wt% platinum). In this region, P25 showed a low level of activity at steady state similar to that of TNW773 not including anatase crystallites (Fig. 9). Similar result of low activity level in the low platinum loading region was confirmed for a commercial titania sample containing both anatase and rutile. On the other hand, photocatalytic activity was saturated at low platinum loading in the case of anatase sample not containing rutile crystallites as shown in Fig. 10c. Ohno et al. have reported that platinum was mainly photodeposited on the rutile rather than anatase in titania powders of well-faceted mixed crystallites [24]. Thus, a low activity level of P25 with platinum loading < 0.4 wt% is expected by selective photodeposition of platinum on the minor rutile phase and

> 0.5 wt% loading might be needed for platinization of the major anatase crystallites. However, it has not been clarified why the initial activity of P25 was relatively high and the H_2 liberation rate decreased with irradiation time.

The liberation of H_2 is promoted over photodeposited platinum particles. Photogenerated positive holes are presumed to be immediately consumed by methanol over the photocatalyst surface. Thus, the electrons left in the photocatalyst must be transferred to the platinum. Recently, Majima et al. have investigated photocatalytic one-electron oxidation of an aromatic compound over titania nanotubes using time-resolved diffuse reflection spectroscopy and reported that the trapped electrons were remarkably long-lived in the nanotubes, when compared to those of nanoparticles [25]. Yanagida et al. have also found that titania nanotube electrodes exhibit a longer electron lifetime than that of an electrode made of P25 particles [26]. These results suggest long diffusion length and excellent transport property of photoinduced electrons in nano-structured titania materials with a high aspect ratio. In the present study, it was found that photocatalytic H_2-liberation rate of TNW973 was saturated even at low platinum loading of ca. 0.05 wt%. However, such saturation of photocatalytic activity at low loading was not characteristic of TNW973, on the basis of results of similar tests for commercial anatase titania samples. Although the nanowires calcined at > 873 K were composites of layered titanate and anatase, the amount of platinum loading was quite low for reaching saturated activity. This indicates that platinum is preferentially deposited on the anatase surface rather than on the titanate surface.

4. Conclusions

Generation of anatase titania crystallites was not necessary for enhancing photocatalytic activities of titanate nanowires except for photocatalytic H_2 liberation; *e.g.*, titanate crystallites with a small amount of defects exhibited considerable photocatalytic activity for O_2 liberation from an aqueous silver sulfate solution and for oxidative decomposition of acetic acid. On the other hand, photocatalytic activity for H_2 liberation from an aqueous methanol solution with *in-situ* deposited platinum was improved only by the generation of anatase crystallites by calcination of titanate nanowires. A chloroplatinic acid was preferentially photodeposited on the anatase surface rather than on the titanate surface in contrast to the composites of anatase and rutile titania. Advantageous

features based on the morphology of the nanowire itself were not found in this study. This might be due to the effects of more significant physical properties, such as composition, crystalline defects and specific surface area, than the nanowire-structured morphologies on the photocatalytic activity and also to the difficulty in changing one structural characteristic with the others remaining unchanged.

References

(1) T. Kasuga, M. Hiramatsu, A. Hoson, T. Sekino and K. Niihara, *Langmuir*, 1998, **14**, 3160.

(2) T. Kasuga, M. Hiramatsu, A. Hoson, T. Sekino and K. Niihara, *Adv. Mater.*, 1999, **11**, 1307.

(3) C. C. Tsai and H. S. Teng, *Chem. Mater.*, 2006, **18**, 367.

(4) J. G. Yu, H. G. Yu, B. Cheng and C. Trapalis, *J. Mol. Catal. A*, 2006, **249**, 135.

(5) J. G. Yu, H. G. Yu, B. Cheng, X. J. Zhao and Q. J. Zhang, *J. Photochem. Photobiol. A*, 2006, **182**, 121.

(6) Y. B. Mao and S. S. Wong, *J. Am. Chem. Soc.*, 2006, **128**, 8217.

(7) A. R. Armstrong, G. Armstrong, J. Canales and P. G. Bruce, *Angew. Chem., Int. Ed.*, 2004, **43**, 2286.

(8) X. M. Sun and Y. D. Li, *Chem. Eur. J.*, 2003, **9**, 2229.

(9) Z. Y. Yuan, X. B. Zhang and B. L. Su, *Appl. Phys. A*, 2004, **78**, 1063.

(10) G.H. Du, Q. Chen, P.D. Han, Y. Yu and L.M. Peng, *Phys. Rev. B*, 2003, **67**, 35323.

(11) X.D. Meng, D.Z. Wang, J.H. Liu, B.X. Lin and Z.X. Fu, *Solid State Commun.*, 2006, **137**, 146.

(12) *Jpn. Pat.*, P2005-162584A, 2005

(13) H. Kominami, J. Kato, Y. Takada, Y. Doushi, B. Ohtani, S. Nishimoto, M. Inoue, T. Inui and Y. Kera, *Catal. Lett.*, 1997, **46**, 235.

(14) H. Kominami, S. Murakami, J. Kato, Y. Kera and B. Ohtani, *J. Phys. Chem. B*, 2002, **106**, 10501.

(15) M. A. Khan, H. T. Jung and O. B. Yang, *J. Phys. Chem. B*, 2006, **110**, 6626.

(16) E. K. Andersen, I. G. K. Andersen and E. Skou, *Solid State Ionics*, 1988, **27**, 181.

(17) T. Torimoto, N. Nakamura, S. Ikeda and B. Ohtani, *Phys. Chem. Chem. Phys.*, 2002, **4**, 5910.

(18) S. Ikeda, N. Sugiyama, S. Murakami, H. Kominami, Y. Kera, H. Noguchi, K. Uosaki, T. Torimoto and B. Ohtani, *Phys. Chem. Chem. Phys.*, 2003, **5**, 778.

(19) B. Ohtani, M. Kakimoto, H. Miyadzu, S. Nishimoto and T. Kagiya, *J. Phys. Chem.*, 1988, **92**, 5773.

(20) M. He, X. Feng, X. H. Lu, X. Y. Ji, C. Liu, N. Z. Bao and J. W. Xie, *J. Mater. Sci.*, 2004, **39**, 3745.

(21) K. S. W. Sing, D. H. Everett, R. A. W. Haul, L. Moscou, R. A. Pierotti, J. Rouquerol and T. Siemieniewska, *Pure Appl. Chem.*, 1985, **57**, 603.

(22) X. T. Gao and I. E. Wachs, *J. Phys. Chem. B*, 2000, **104**, 1261.

(23) X. Yan, T. Ohno, K. Nishijima, R. Abe and B. Ohtani, *Chemi. Phys. Lett.*, 2006, **429**, 606.

(24) T. Ohno, K. Sarukawa and M. Matsumura, *New J. Chem.*, 2002, **26**, 1167.

(25) T. Tachikawa, S. Tojo, M. Fujitsuka, T. Sekino and T. Majima, *J. Phys. Chem. B*, 2006, **110**, 14055.

(26) Y. Ohsaki, N. Masaki, T. Kitamura, Y. Wada, T. Okamoto, T. Sekino, K. Niihara and S. Yanagida, *Phys. Chem. Chem. Phys.*, 2005, **7**, 4157.

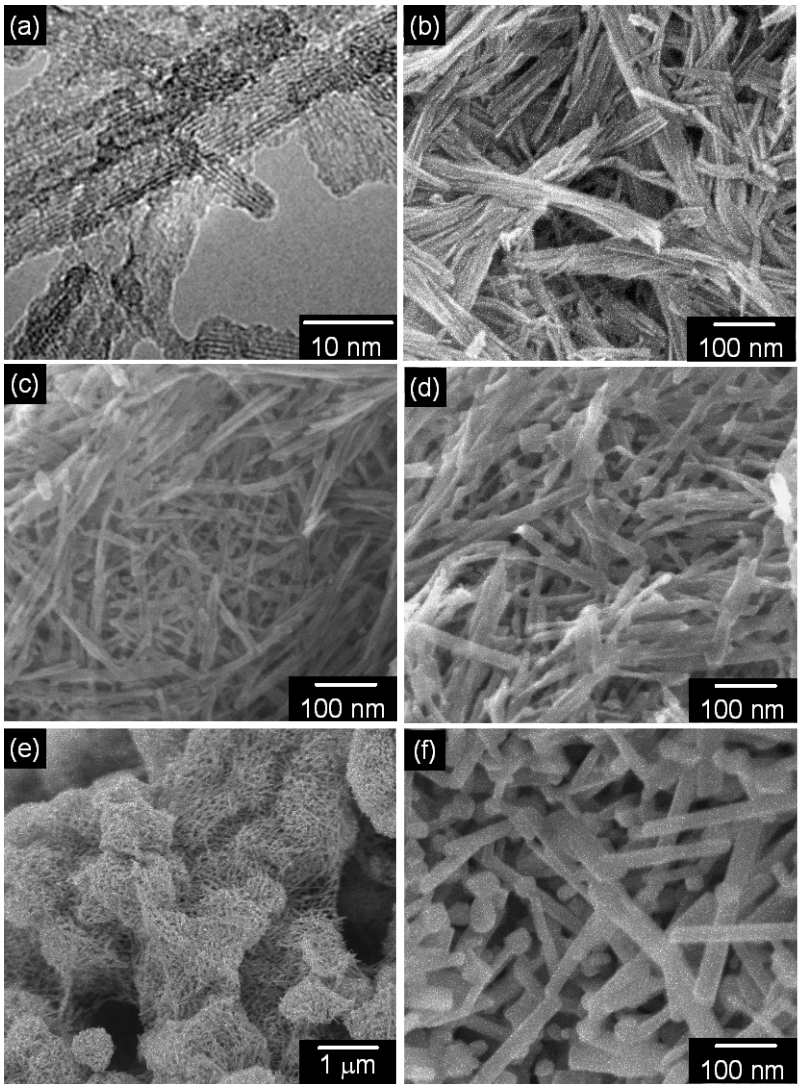

Figure 1. (a) TEM image of TNW0 and FE-SEM images of (b) TNW0, (c) TNW773, (d) TNW873, (e) TNW973 in low magnification, and (f) TNW973.

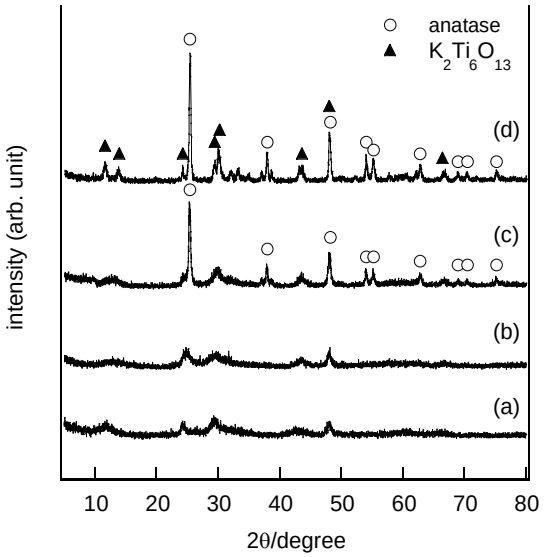

Figure 2. XRD patterns of (a) TNW0, (b) TNW773, (c) TNW873, and (d) TNW973.

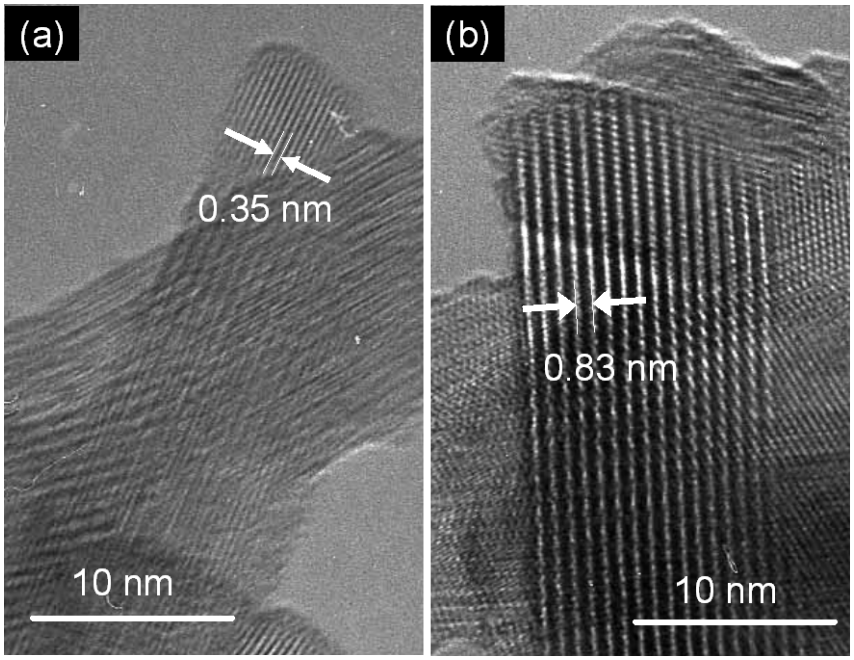

Figure 3. TEM images of nanowire-structured (a) anatase titania and (b) layered titanate in TNW873.

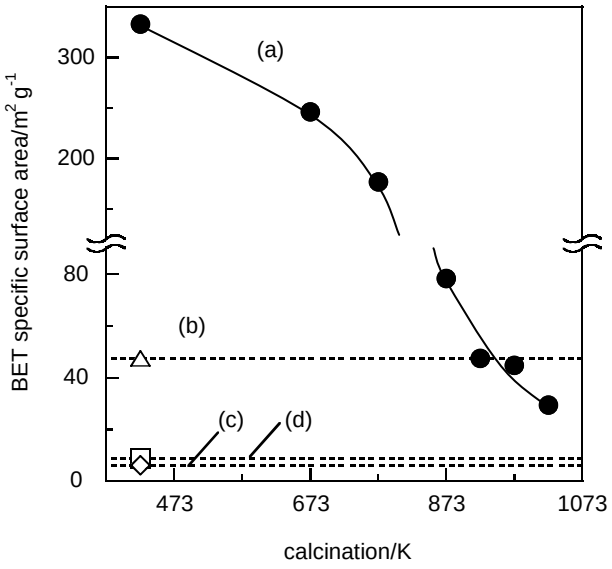

Figure 4. BET specific surface areas of (a) TNW, (b) P25, (c) $K_2Ti_4O_9$, and (d) $K_2Ti_6O_{13}$. The x-axis refers to the calcination temperature of TNW samples only.

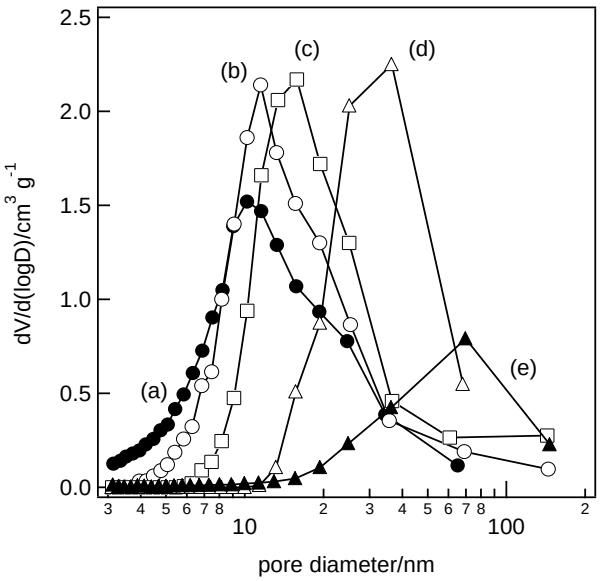

Figure 5. Pore volume distributions (plot of log-differential pore volume versus pore diameter) of (a) TNW0, (b) TNW673, (c) TNW773, (d) TNW873, and (e) TNW973.

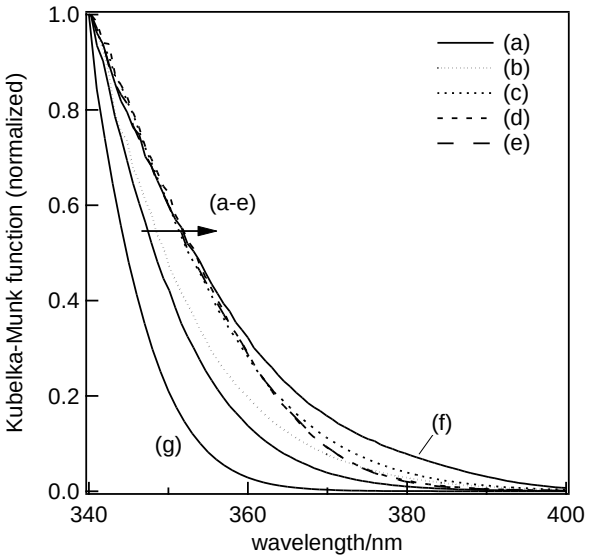

Figure 6. Diffuse reflection electronic spectra of (a) TNW0, (b) TNW673, (c) TNW773, (d) TNW873, (e) TNW973, (f) P25, and (g) $K_2Ti_6O_{13}$. The Kubelka-Munk functions were normalized by the intensity at 340 nm.

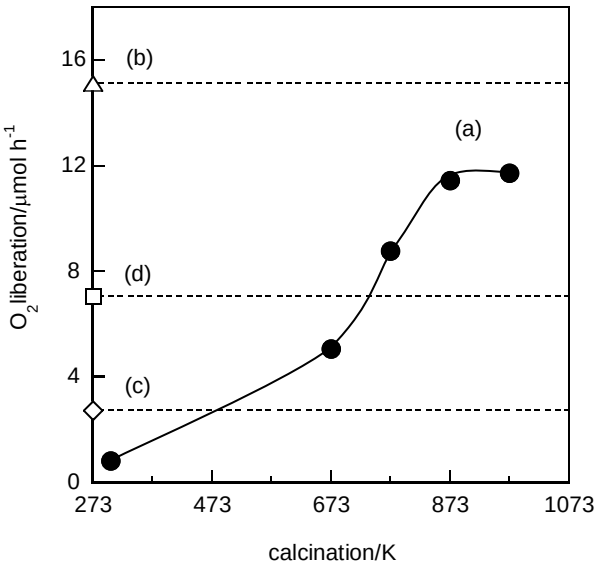

Figure 7. Rate of oxygen liberation in the photocatalytic oxidation of water over (a) TNW, (b) P25, (c) $K_2Ti_4O_9$, and (d) $K_2Ti_6O_{13}$. The x-axis refers to the calcination temperature of TNW samples only.

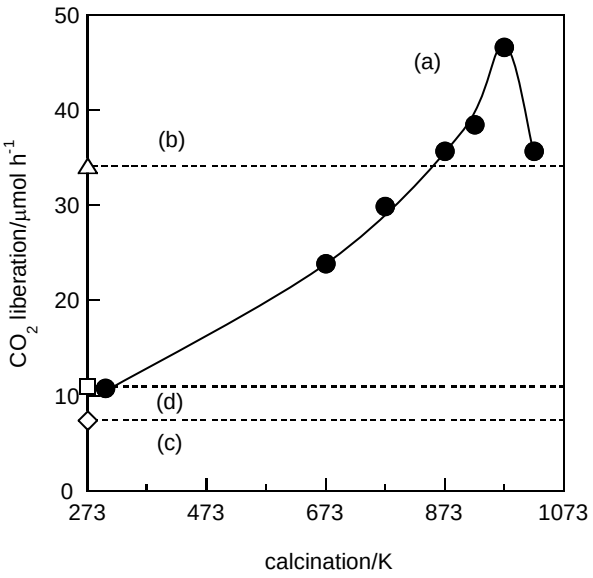

Figure 8. Rate of carbon dioxide liberation in the photocatalytic oxidative decomposition of acetic acid over (a) TNW, (b) P25, (c) $K_2Ti_4O_9$, and (d) $K_2Ti_6O_{13}$. The x-axis refers to the calcination temperature of TNW samples only.

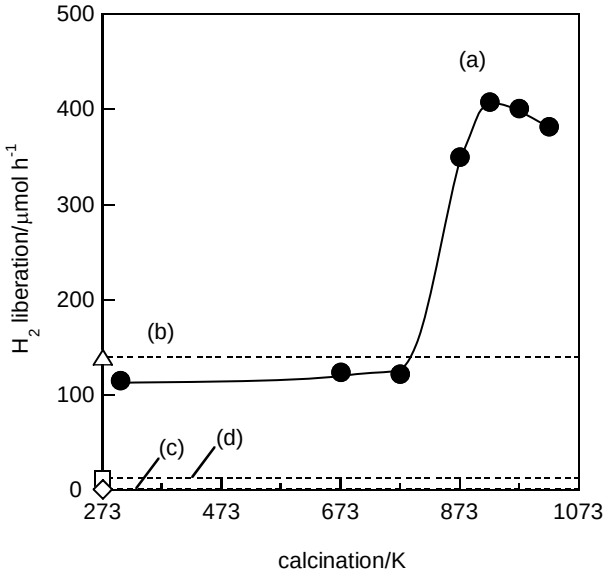

Figure 9. Rate of photocatalytic hydrogen liberation from an aqueous methanol solution over (a) TNW, (b) P25, (c) $K_2Ti_4O_9$, and (d) $K_2Ti_6O_{13}$. The amount of platinum was adjusted to 0.1 wt% as metal. The x-axis refers to the calcination temperature of TNW samples only.

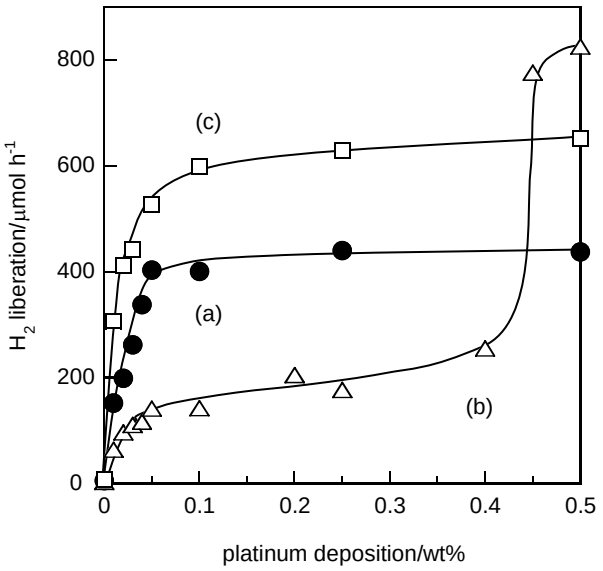

Figure 10. Effect of platinum loading on the photocatalytic hydrogen liberation from an aqueous methanol solution over (a) TNW973, (b) P25, and (c) anatase titania JRC-TIO-13 supplied by the Catalysis Society of Japan.